https://doi.org/10.52676/1729-7885-2026-2-131-141
УДК 535.37

STUDY OF THE LUMINESCENT CHARACTERISTICS OF PURE AND FLUORINE-CONTAINING BIO-HYDROXYAPATITE

K. B. Zhangylyssov, D. H. Daurenbekov, T. T. Alibay, G. B. Bairbayeva, A. S. Akhmetova, R. K. Daurenbekova, B. N. Yussupbekova, Y. G. Koshkinbayev, A. Talgatuly*

L.N. Gumilyov Eurasian National University

** E-mail for contacts: adil.talgatuly.00@gmail.com*

This work presents a comparative study of pure and fluorine-containing hydroxyapatite (HAp and HAp–F), focusing on the effect of fluoride ions on the structural and optical properties of the material. The samples were synthesized using a rapid pyrolysis method and characterized by X-ray diffraction (XRD), Fourier-transform infrared spectroscopy (FTIR), and luminescence spectroscopy. XRD analysis showed that both materials crystallize in a hexagonal apatite structure with the space group $P6_3/m$. The FTIR and XRD data suggest structural changes associated with the partial incorporation of F^- ions and modifications in the local environment of phosphate groups. The spectral and luminescence measurements revealed that the presence of fluorine affects the luminescence behavior, including changes in the visible spectral region and possible modification of energy-transfer processes. Overall, these findings show that the incorporation of fluorine influences the structural and optical properties of hydroxyapatite and may provide a basis for further studies of apatite-based materials for biomedical and luminescent applications.

Keywords: *Hydroxyapatite; fluorine-modified hydroxyapatite; fluorohydroxyapatite; infrared spectroscopy; X-ray diffraction; scanning electron microscopy; elemental analysis; photoluminescence.*

Introduction

Biogenic and synthetic hydroxyapatite are crystallochemically variable materials whose properties are governed by their composition, degree of crystallinity, and surface state. Biogenic HAp can be obtained from tooth enamel, with its phase composition controlled by heat treatment. Subsequent ionic modification, such as Cu^{2+}/Ag^+ incorporation, leads to reproducible structural and morphological changes detectable by X-ray diffraction. Fourier-transform infrared spectroscopy, and scanning electron microscopy (SEM). [1] Similarly, the stable production of nano-HAp from biogenic sources while maintaining phase purity and defined crystallinity confirms the feasibility of targeted control over the structural parameters of biogenic apatites. [2]

Ionic incorporation in the HAp lattice, even at the level of a few percent, causes measurable changes in lattice parameters, crystallinity, and surface characteristics, such as ζ-potential and ion exchange. This provides an experimental basis for comparing pure and modified forms of apatite. [3] At the coating level, variations in crystallinity and apatite-phase structure have been shown to cause significant changes in functional properties. [4] Overall, ionic modification is regarded as a versatile tool for tailoring the crystallochemistry, morphology, and solubility of HAp. Therefore, analyzing the influence of specific ionic modifications, including fluorine-related modification, on measurable material responses is methodologically and physically justified. [5] The wide range of permissible incorporations in the HAp structure is exploited in the design of functional coatings and hybrid systems, further motivating investigation of the role of F^- ions in bio-HAp. [6]

When comparing HAp modifications, microstructural and surface parameters must be controlled because the functional properties of nano-HAp depend on morphology, specific surface area, charge, and electrical conductivity. [7] To improve reproducibility, standardized synthetic enamel-like HAp surfaces are used as model substrates for comparative studies. [8] Methodological limitations should also be considered: crystallite size estimation from XRD strongly depends on the selected model, while approaches such as the Monshi–Scherrer method show better agreement with Brunauer–Emmett–Teller surface area analysis and transmission electron microscopy, with lower systematic errors. [9]

The practical relevance of modified apatites is supported by the widespread use of nano-HAp in dental composites as a functional filler and delivery platform, including for sealing dentinal tubules and suppressing bacterial growth. [10] The incorporation of nano-HAp into dental nanocomposites increases bioactivity and biocompatibility and may enhance antibacterial performance. This requires reproducible control of apatite-phase properties during compositional modification. [11] At the same time, assessing the biological safety of nanoparticles and the factors governing their interactions with biosystems remains an important task. [12] In bone tissue engineering, nano-HAp is also used as a component of composite scaffolds and as a carrier for bioactive factors and drugs. [13]

Alongside regenerative applications, multifunctional HAp systems are being developed with optical and diag-

nostic capabilities. The integration of fluorescent components and theranostic nanoplatforms into HA scaffolds highlights the need for an optical response, including luminescence, in apatite-based materials. [14] The expansion of HAp applications into bioimaging and functional coatings further increases the need to correlate compositional modifications and defect structure with spectral characteristics. [15] More broadly, inorganic nanoparticles, including HAp, are considered promising delivery and bioimaging platforms because of their combined physicochemical and optical properties. [16]

Because of its limited mechanical properties, HAp is often used in composites and functional coatings. This increases the need to control the structure and properties of the apatite component during modification. [17] In composite scaffolds, matrix degradation and exposure of the apatite phase are critical because they determine ion exchange and bioactivity. These factors should therefore be considered when interpreting results for modified apatites. [18] In addition, the development of composites with physical effects, such as electrical conductivity and the transmission of endogenous electrical signals, emphasizes that structural tuning of HAp is a key determinant of system functionality. [19]

Recent studies have shown that fluorine modification of hydroxyapatite can be directed toward different functional purposes. For example, in a recent work, a composition-graded core–shell HAP@FAP structure was prepared by surface-gradient F-doping in order to introduce a built-in strain gradient and enhance the flexoelectric/piezoelectric response for piezocatalytic degradation of phenanthrene in soil. Thus, in that study, fluorine incorporation was mainly considered as a tool for creating a heterostructured piezocatalyst with improved mechanical-energy-driven catalytic activity. In contrast, the present work focuses on a simpler comparative system of pure HAp and fluorine-containing HAp–F, where the main objective is to clarify how F^- incorporation affects the apatite structure and luminescent behavior. This distinction is important because the influence of fluorine-related structural changes on the visible luminescence response of HAp remains less systematically discussed compared with catalytic, piezoelectric, and biomedical aspects of fluorinated apatites.

Therefore, studying the luminescent characteristics of pure and fluorine-containing hydroxyapatite derived from biogenic sources is a well-founded approach for identifying correlations of the type “fluorine-related modification–defect structure–microstructure spectral response” and for establishing criteria for spectroscopic monitoring of modified apatite materials. The scientific novelty of this work lies in the comparative analysis of HAp and HAp–F obtained under the same synthesis conditions, with emphasis on the relationship between F^- incorporation, structural changes detected by XRD and FTIR, and changes in the luminescence response. [20]

The objective of this work is to compare the structural, vibrational, morphological, and luminescent properties of pure biogenic hydroxyapatite and fluorine-containing hydroxyapatite synthesized under identical conditions, with particular attention to the relationship between F^- incorporation, defect-related states, and visible luminescence.

Samples and Methods

Biogenic hydroxyapatite was synthesized using a rapid pyrolysis method. Raw bovine bones were used as the starting material. First, the organic component was removed, and the samples were dried. The resulting material was then calcined at 750 °C. The obtained samples were ground in a mortar, and fluorine-containing components were introduced using a solvation–precipitation approach. The powders prepared for luminescence measurements were pressed into copper sample holders with a thickness of 0.5 mm and a diameter of approximately 10 mm. Pressing was carried out using a manual press at approximately 0.1…0.2 MPa. The resulting powders were characterized by photoluminescence spectroscopy, infrared spectroscopy, and X-ray diffraction. Scanning electron microscopy images were obtained using a Hitachi TM4000 microscope operated in backscattered electron (BSE) mode. The SEM measurements were carried out at an accelerating voltage of 15 kV under different magnification conditions. SEM analysis was used to examine the surface morphology and particle/agglomerate characteristics of the synthesized powders.

Luminescence measurements were performed over the spectral range of 200…700 nm using a Solar CM 2203 spectrofluorimeter. The molecular structure was examined in the range of 400…4000 cm^{-1} using a Jasco IR-4700 spectrometer equipped with an attenuated total reflection (ATR) module. Structural and phase analyses were performed on a Bruker D6 Phaser diffractometer in the 2θ range of 10…80°.

Results and Discussion

Infrared spectroscopy was carried out to study the structural features of pure HAp and fluorine-modified hydroxyapatite. The IR spectra of both samples are presented together in Figure 1, and the main absorption bands with their assignments are summarized in Table 1. This comparison makes it possible to evaluate the changes in the apatite structure after fluorine incorporation.

As shown in Figure 1, both HAp and HAp–F exhibit the characteristic absorption bands of the apatite phase. The intense bands in the region of 1096…1036 cm^{-1} correspond to the asymmetric stretching vibrations of phosphate groups, $\nu_3(PO_4^{3-})$. The band at 962…964 cm^{-1} is assigned to the symmetric stretching vibration of phosphate groups, $\nu_1(PO_4^{3-})$. The bands observed at 604…569 cm^{-1} are attributed to the bending vibrations of phosphate groups, $\nu_4(PO_4^{3-})$. The presence of these bands in both spectra confirms that the apatite structure is preserved after fluorine modification.

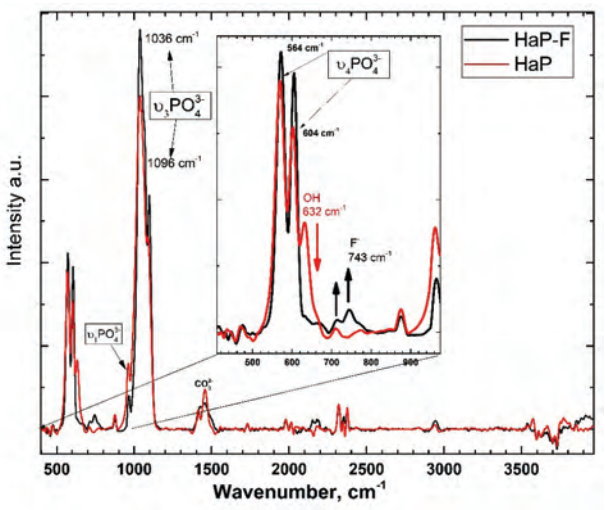

Figure 1. IR spectrum of pure hydroxyapatite and fluorine-modified hydroxyapatite.

For the initial HAp sample, the band near 636 cm^{-1} is associated with the librational vibration of structural hydroxyl groups, OH^-, located in the apatite channels. After fluorine modification, this band decreases in intensity, as also indicated in Table 1. This change suggests partial substitution of hydroxyl groups by fluoride ions in the apatite structure.

A notable feature of the HAp–F spectrum is the appearance or intensification of absorption in the 700…750 cm^{-1} region. This band is related to interactions in the fluorohydroxyapatite channels and can be associated with structural changes caused by the incorporation of F^- ions. Therefore, the increase in this region, together with the decrease of the OH^- libration band near 636 cm^{-1}, confirms the formation of fluorine-containing hydroxyapatite.

A slight shift of the phosphate band from 962 cm^{-1} in HAp to 964 cm^{-1} in HAp–F is also observed. This shift may be attributed to local distortion of phosphate groups due to fluorine incorporation into the apatite lattice. In addition, the phosphate stretching region around 1096–1036 cm^{-1} remains clearly visible in both samples, indicating that fluorine modification does not destroy the apatite framework.

Table 1. IR spectra of HAp and HAp–F samples

Wavenumber, cm^{-1}	Assignment	Interpretation
1036–1096	$v_3\ PO_4^{3-}$	phosphate stretching
962–964	$v_1\ PO_4^{3-}$	local distortion of phosphate groups
564–604	$v_4\ PO_4^{3-}$	apatite phase confirmation
636	OH^- libration	decreases after F modification
700-750	F^-	interactions in fluorohydroxyapatite channels, increases after F modification
1411–1456	CO_3^{2-}	carbonate substitution/adsorption

The bands in the region of 1456…1411 cm^{-1} are attributed to carbonate groups, CO_3^{2-}. Their presence indicates carbonate substitution or adsorption in the apatite structure. This is typical for bio-derived hydroxyapatite and suggests that the obtained material is not completely stoichiometric HAp, but rather carbonate-containing apatite.

Thus, the combined analysis of Figure 1 and Table 1 shows that the main phosphate bands of hydroxyapatite are retained after fluorine modification, confirming the preservation of the apatite phase. At the same time, the decrease of the OH^- band near 636 cm^{-1} and the increase of the band in the 700…750 cm^{-1} region indicate the incorporation of fluoride ions into the apatite channels. These spectral changes confirm the successful formation of fluorine-modified hydroxyapatite while maintaining the basic apatite structure.

SEM analysis was performed to evaluate the morphology of the fluorine-containing hydroxyapatite sample after modification. The SEM images of the HAp–F powder are presented in Figure 2. The sample

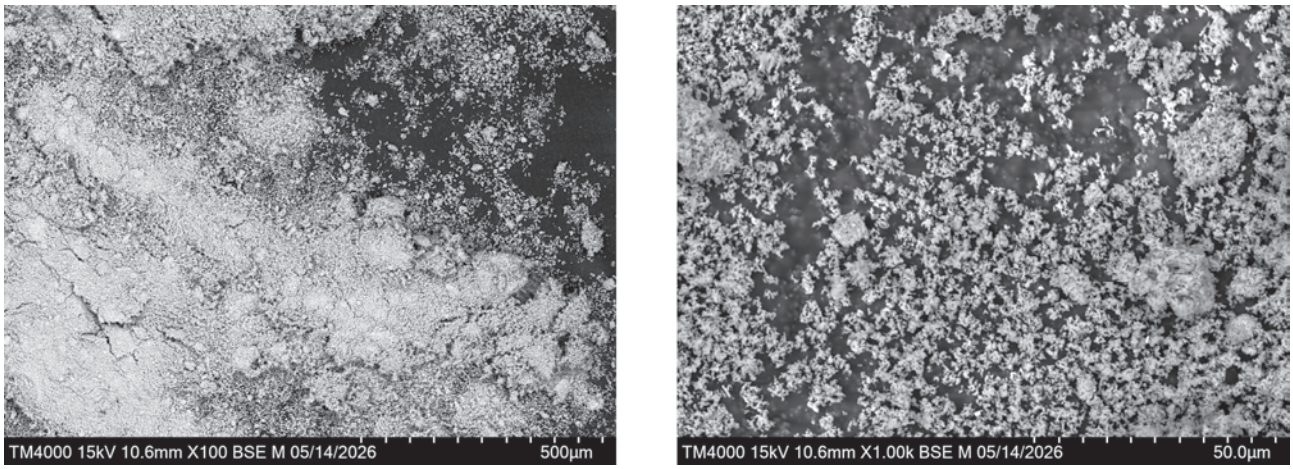

Figure 2. SEM images of the HAp–F sample

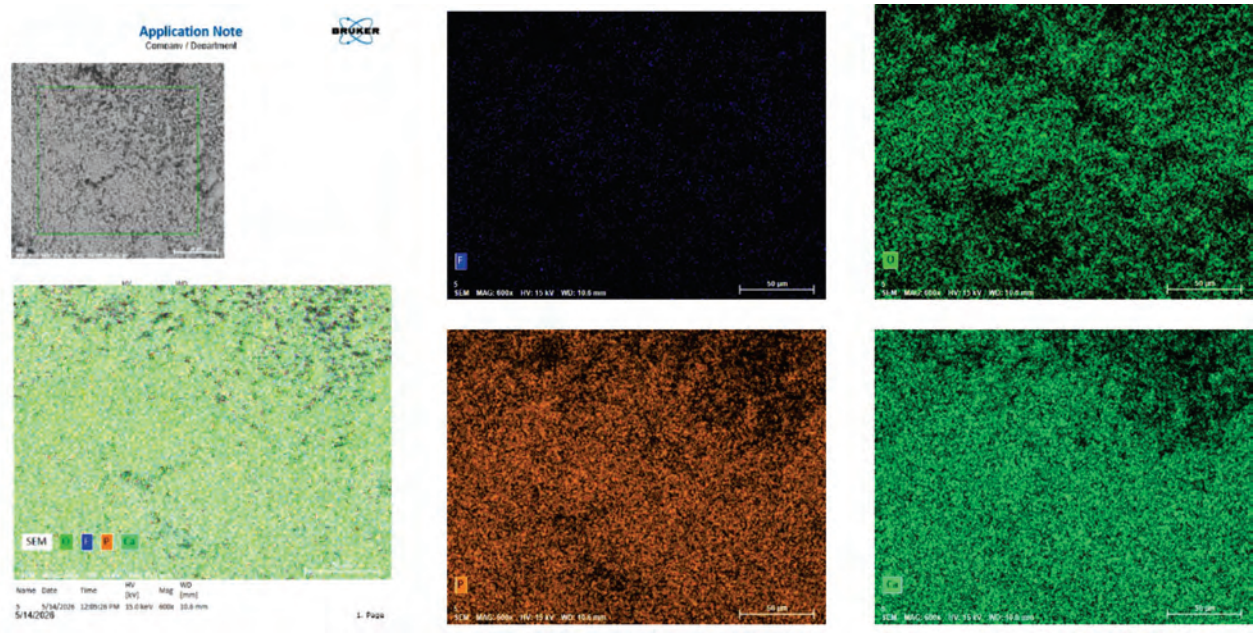

Figure 3. SEM–EDX elemental mapping of the HAp–F sample

demonstrates an agglomerated morphology consisting of irregularly shaped particles and compact aggregates. The particles are distributed non-uniformly over the surface, forming clusters of different sizes. At higher magnification, individual particle fragments with sizes of approximately 1.2–2.0 μm can be distinguished.

The observed morphology is typical for thermally treated calcium phosphate powders. The formation of dense agglomerates may be associated with calcination, partial sintering of particles, and subsequent grinding of the powder. Such agglomeration is also characteristic of hydroxyapatite-based materials due to their high surface energy and tendency of fine particles to form secondary aggregates.

SEM–EDX mapping was carried out to evaluate the elemental distribution in the HAp–F sample, as shown in Figure 3. The mapping results confirm the presence of the main elements associated with fluorine-containing hydroxyapatite, including calcium, phosphorus, oxygen, and fluorine. The distribution of these elements over the analyzed region indicates that fluorine is incorporated into the material rather than being present only as a separate localized impurity. This supports the formation of a fluorine-modified hydroxyapatite phase.

The EDX scanning results shown in Figure 4 further confirm the elemental composition of the HAp–F sample. The detection of calcium and phosphorus corresponds to the apatite matrix, while the presence of fluorine confirms successful fluorine modification. The simultaneous presence of Ca, P, O, and F is consistent with the formation of fluorohydroxyapatite or fluorine-substituted hydroxyapatite. However, since EDX provides mainly local elemental information, the incorporation of fluorine into the apatite lattice should be interpreted together with the IR spectroscopy results, where changes in the OH^-- and F^--sensitive regions were observed.

Thus, SEM analysis shows that the HAp–F sample has an agglomerated powder morphology with irregular particle shape and micron-sized fragments. The EDX mapping and scanning results confirm the presence and distribution of fluorine in the hydroxyapatite-based material. These findings support the successful modification of hydroxyapatite with fluorine while preserving the typical morphology of thermally treated calcium phosphate powders.

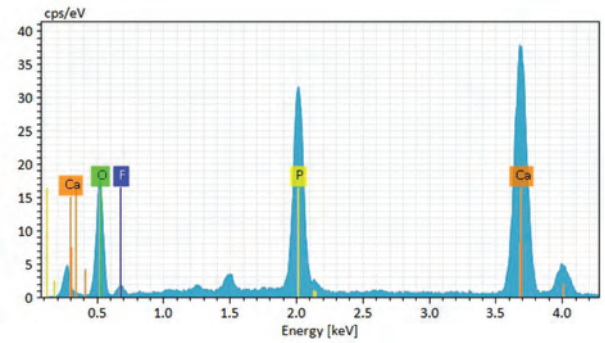

Figure 4. SEM–EDX spectrum/scanning analysis of the HAp–F sample

To investigate the crystalline structure of the synthesized hydroxyapatite (HAp) and fluorine-containing hydroxyapatite samples, X-ray diffraction analysis was performed over the 2θ range of 10…80°. Figures 5 and 6 show the experimental diffraction patterns of the samples together with the reference reflection profiles from the Powder

Diffraction File (PDF) database for hydroxyapatite (PDF No. 86-0740) and fluorapatite (PDF No. 15-0876).

The diffraction pattern of pure hydroxyapatite shows distinct high-intensity diffraction peaks corresponding to the crystalline $Ca_5(PO_4)_3(OH)$ phase characteristic of hydroxyapatite. The dominant reflections are recorded at $2\theta \approx 25.8°$, 31.8°, 32.9°, 34.0°, 39.8°, 46.7°, 49.5°, 53.2°, and 64.0°, which agrees well with the PDF 86-0740 reference data. The high intensity and narrow shape of the peaks indicate a high degree of crystallinity of the synthesized material. The absence of additional or extraneous peaks suggests that no secondary crystalline phases were detected within the sensitivity of the XRD method.

Hydroxyapatite crystallizes in a hexagonal crystal system with the space group $P6_3/m$.

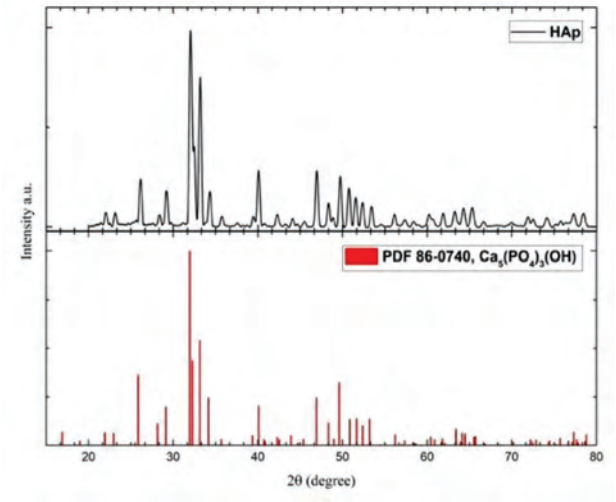

Figure 5. X-ray diffraction (XRD) pattern of pure hydroxyapatite (HAp).

For fluorine-containing hydroxyapatite, the diffraction pattern also shows distinct sharp peaks; however, their positions and relative intensities are slightly altered compared with those of pure HAp. The dominant peaks are close to the reference reflections of fluorapatite $Ca_5(PO_4)_3F$ according to PDF 15-0876. The shift of some peaks toward higher 2θ values may be associated with the incorporation of fluorine into the apatite structure and the corresponding changes in interplanar distances. This shift may be related to the smaller effective size of fluoride ions (F^-) compared with that of hydroxyl groups (OH^-), which may contribute to local structural rearrangement in the apatite lattice.

The HAp–F sample also exhibits a hexagonal apatite-type structure with the space group $P6_3/m$. The reference unit-cell parameters for fluorapatite are slightly smaller than those of hydroxyapatite: $a = b \approx 9.367$ Å and $c \approx 6.884$ Å. Therefore, the observed shift of the diffraction peaks in HAp–F is consistent with structural changes expected for fluorine-containing apatite phases, while the overall lattice symmetry remains preserved.

The XRD results show that the synthesized hydroxyapatite has a high degree of crystallinity. The absence of additional pronounced diffraction peaks suggests that no secondary crystalline phases were detected within the sensitivity of the XRD method. Fluorine modification leads to the formation of a fluorine-containing apatite phase without clearly detectable secondary phases, suggesting structural changes associated with fluorine incorporation.

Overall, X-ray diffraction analysis showed that both samples — pure hydroxyapatite and fluorine-containing hydroxyapatite — possess the hexagonal apatite-type structure with the space group $P6_3/m$. The observed shifts of the diffraction peaks suggest changes in interplanar distances and support the incorporation of fluorine without disrupting the primary apatite crystal structure.

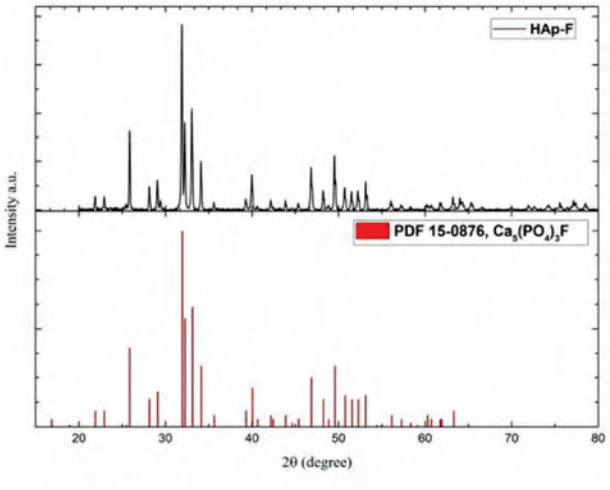

Figure 6. X-ray diffraction (XRD) pattern of fluorine-doped hydroxyapatite (HAp–F).

To further evaluate the agreement between the experimental diffraction data and the reference PDF patterns, the deviation of the peak positions was calculated as $\Delta 2\theta = 2\theta exp - 2\theta PDF$ (Table 2). For the HAp sample, the average absolute deviation from the hydroxyapatite reference pattern PDF 86-0740 was approximately 0.126°, while for the HAp–F sample the average absolute deviation from the fluorapatite reference pattern PDF 15-0876 was approximately 0.051°. The smaller deviation observed for HAp–F indicates a good correspondence between the experimental pattern and the fluorapatite reference structure. This result supports the formation of a fluorine-containing apatite phase after fluorine modification.

Most of the HAp–F diffraction peaks are slightly shifted to lower 2θ values compared with the fluorapatite reference data, with an average shift of approximately −0.047°. Such small shifts may be associated with lattice distortion, partial substitution of OH^- by F^-, carbonate incorporation, and local compositional variations in the apatite structure. At the same time, the absence of additional intense peaks indicates that no pronounced second-

ary crystalline phases were detected within the sensitivity of the XRD method.

For clarity, only the main diagnostic diffraction peaks of the HAp and HAp–F samples are presented in Table 2. These reflections were selected because they correspond to the most intense and characteristic peaks of the apatite structure and are sufficient for phase identification.

Table 2. Comparison of XRD peak positions of HAp and HAp–F samples

HAp, 2θ	HAp PDF 86-0740, 2θ	HAp–F, 2θ	HAp–F PDF 15-0876, 2θ	Assignment / significance
26.15	25.872	25.44	25.473	characteristic apatite reflection
32.05	32.275	31.89	31.937	main apatite peak
33.18	33.157	32.22	32.268	main apatite peak
34.30	34.167	33.07	33.128	apatite structure confirmation
39.44	39.364	39.28	39.330	apatite reflection
46.92	46.947	46.86	46.866	apatite reflection
49.73	49.620	49.54	49.584	apatite reflection
53.42	53.195	53.12	53.145	apatite reflection

To investigate electronic transitions in hydroxyapatite and fluorine-containing hydroxyapatite, excitation (Ex) and emission (Em) spectra were recorded using a CM2203 spectrofluorimeter. These spectra make it possible to identify characteristic energy levels, electronic transitions, and possible energy-transfer processes within the material structure.

To study the luminescent properties of hydroxyapatite, the sample was excited in the wavelength range of 200–220 nm (Figure 7). Two dominant bands were recorded in the excitation spectrum, corresponding to intense luminescence bands in the regions around 340 and 450 nm. Under excitation at 200 nm, the spectrum shows a broad intensity distribution in the ultraviolet and blue regions, suggesting the excitation of high-energy states associated with defects in the crystal lattice.

Under excitation at 220 nm, a predominantly single intense luminescence maximum is observed, suggesting more selective excitation of specific states involved in energy relaxation. According to the literature, emission in the ~450 nm region is associated with the dominant transition in the hydroxyapatite system.

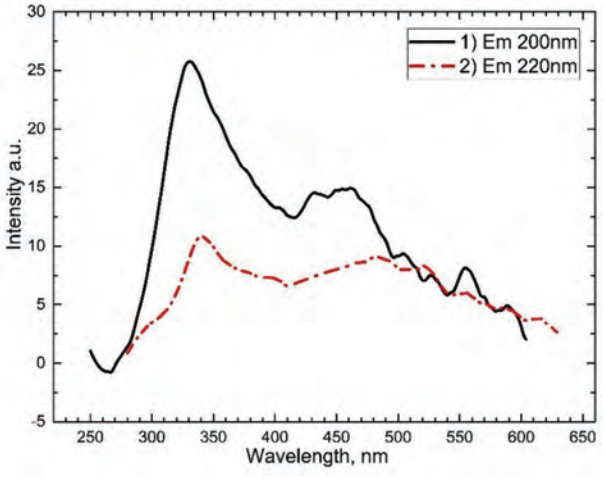

Figure 7. Emission spectra recorded under excitation at 200 and 220 nm.

Subsequently, excitation spectra were recorded for the emission bands at 340 and 450 nm (Figure 8).

In the excitation spectrum corresponding to the 340 nm emission band (Figure 8a), bands in the 200–260 nm range are observed. These bands suggest the excitation of high-energy states that may be associated with defect levels, such as oxygen vacancies or structural distortions of PO_4^{3-} groups. Excitation by short-wavelength photons may lead to relaxation to localized states, followed by photon emission at 340 nm.

For the 450 nm emission band (Figure 8b), excitation bands were registered at 260, 335, and 365 nm. These

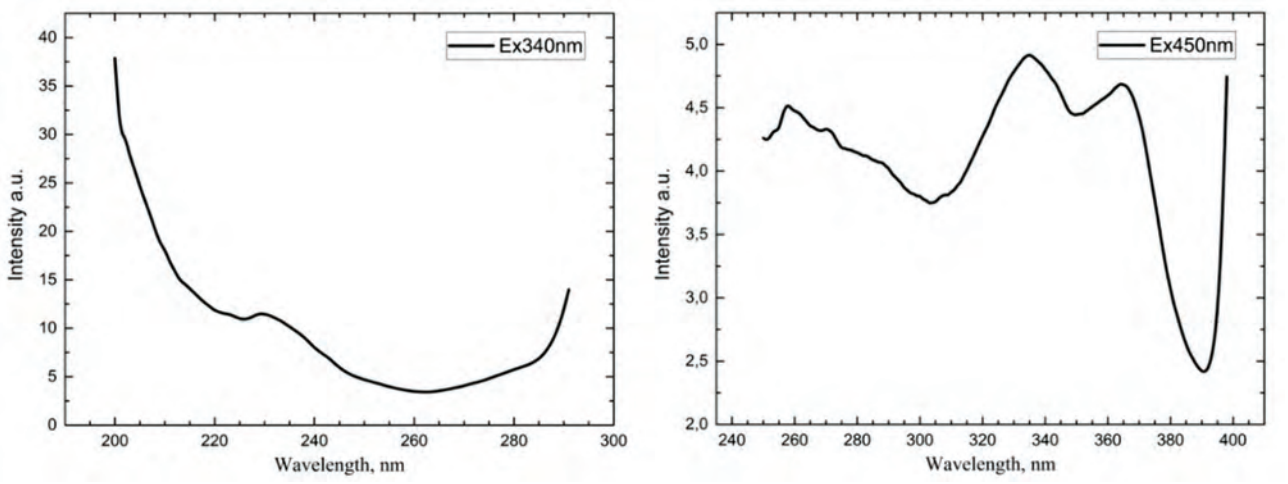

Figure 8. Excitation spectra for the emission bands at 340 nm (a) and 450 nm (b).

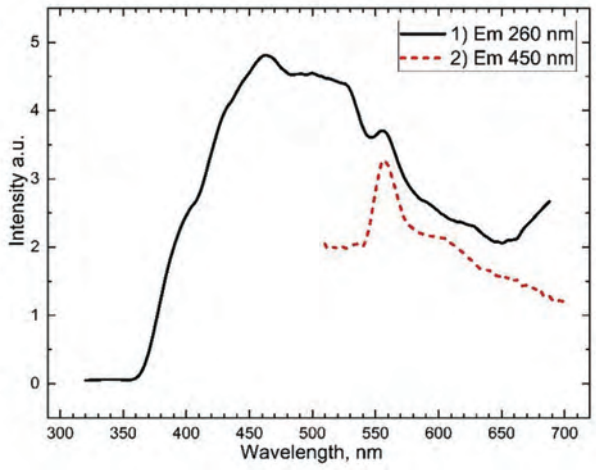

Figure 9. Emission spectra recorded under excitation at (a) 260 and (b) 450 nm.

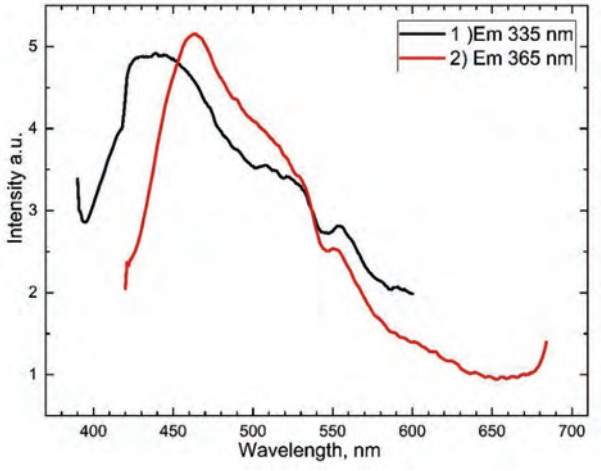

Figure 10. Emission spectra recorded under excitation at (a) 335 nm and (b) 365 nm.

data suggest a possible multistep relaxation process, in which excitation to higher-energy levels may be followed by energy transfer to defect-related states and subsequent emission at 450 nm.

As discussed earlier, under excitation at 260 nm (Fig. 9, line a), broadband luminescence was recorded, consisting of several emission components and spanning the 370…650 nm range. Within this range, dominant emission bands were identified at approximately 374, 450, and 555 nm. Such a spectral structure suggests the excitation of high-energy states followed by relaxation through several possible intermediate defect-related levels.

Under excitation at 450 nm (Figure 9, line b), selective enhancement of the emission band at 450 nm is observed, which may indicate energy redistribution between the corresponding electronic states.

Under excitation at 335 nm (Figure 10, line a), the emission spectrum exhibits a maximum at 426 nm. This may be associated with electronic transitions involving excited states near the valence-band edge and localized defect-related states.

A similar pattern is observed under excitation at 365 nm (Figure 10, line b), supporting the presence of defect-related energy levels contributing to emission in the blue region of the spectrum. In the spectra shown in Figure 10, the dominant luminescence bands in the regions around 450 and 555 nm are clearly observed.

The excitation spectrum recorded for the 555 nm emission band shows an intense maximum at 450 nm, supporting a correlation between the corresponding energy levels (Figure 11). This observation suggests a possible multistep energy-transfer process, in which excitation in the blue region is followed by relaxation and photon emission in the green region (~555 nm).

To investigate the luminescent properties of fluorine-containing hydroxyapatite, the sample was excited at various wavelengths, and the corresponding emission spectra were recorded. Under excitation at 220 nm,

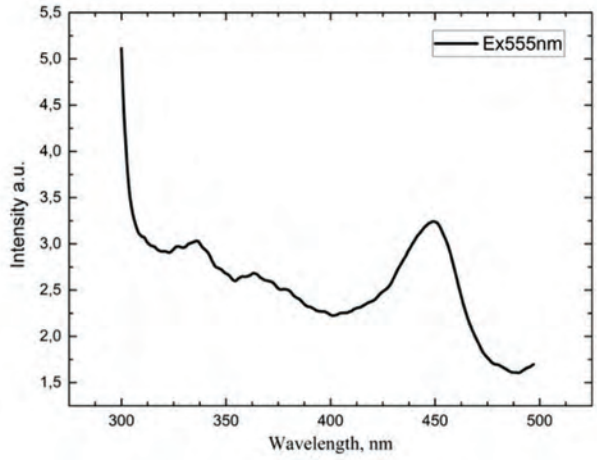

Figure 11. Excitation spectrum of pure HAp monitored at 555 nm emission.

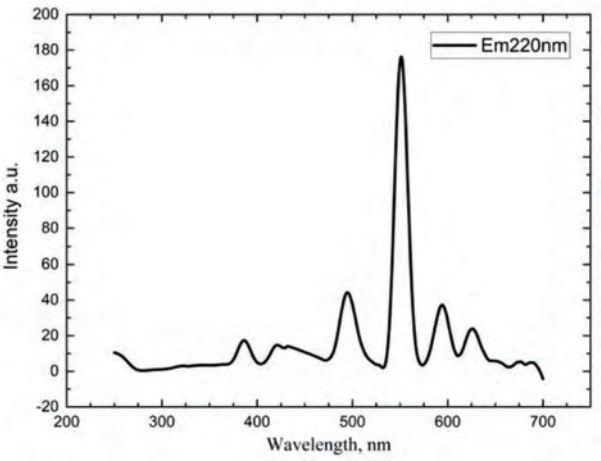

Figure 12. Emission spectrum of HAp–F recorded under excitation at 220 nm.

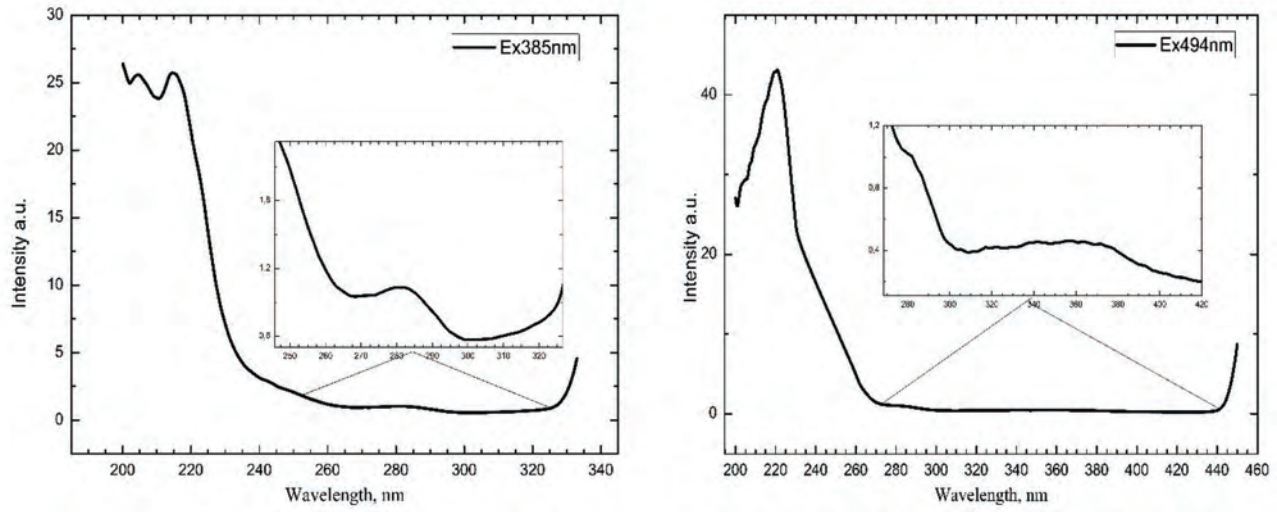

Figure 13. Excitation spectra of HAp–F for the emission bands at (a) 385 nm and (b) 494 nm.

intense emission bands were observed at 385, 494, 550, 594, and 625 nm (Figure 12). The relationship between the excitation conditions and the emission spectra suggests changes in the luminescence behavior associated with the incorporation of fluoride ions into the crystal lattice. The observed band distribution indicates possible modification of defect-related electronic states associated with fluorine incorporation in the hydroxyapatite lattice.

Further analysis focused on the excitation spectra recorded for the emission bands at 385 and 494 nm. For the 385 nm emission band, the excitation spectrum shows pronounced bands in the ~220 nm region (Figure 13a), suggesting efficient excitation of high-energy states followed by relaxation to the level responsible for emission at 385 nm. For the 494 nm emission band, the excitation spectrum exhibits bands at 318, 355, and 372 nm (Figure 13b), suggesting a possible multistep energy-transfer process between defect-related states associated with fluorine incorporation.

Under excitation of the HAp–F sample at 318 nm (Figure 14a), broad composite luminescence bands were observed in the regions around 420 and 550 nm. These results suggest that the excitation energy influences electronic transitions in the material and reflects the complex nature of energy-transfer processes. Under excitation at 355 (Figure 14b) and 372 nm (Figure 14c), emission bands were also observed in the regions around 420 and 550 nm. The presence of these maxima under different excitation wavelengths supports the involvement of stable energy states in the luminescence processes and suggests energy transfer between various defect-related levels.

In summary, the excitation spectrum recorded for the 550 nm emission band reproduced the previously observed excitation bands at 318, 355, and 372 nm (Figure 15). The repeated appearance of these excitation maxima supports the presence of reproducible excitation features and possible energy-transfer processes in the HAp–F structure

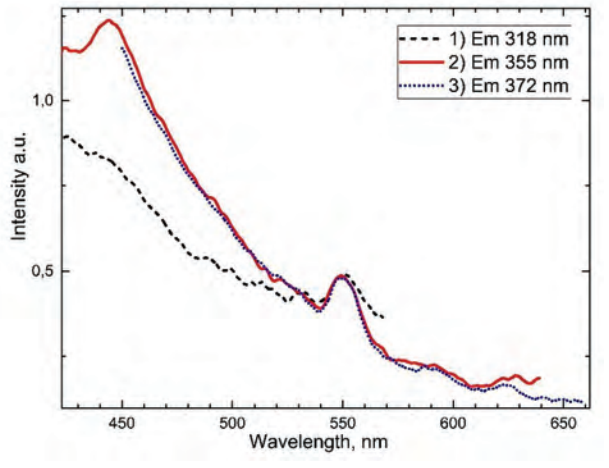

Figure 14. Emission spectra recorded under excitation at (a) 318 nm, (b) 355 nm, and (c) 372 nm.

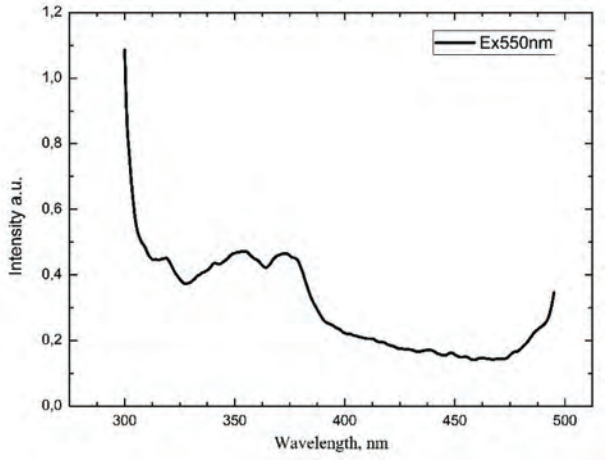

Figure 15. Excitation spectrum monitored at 550 nm emission.

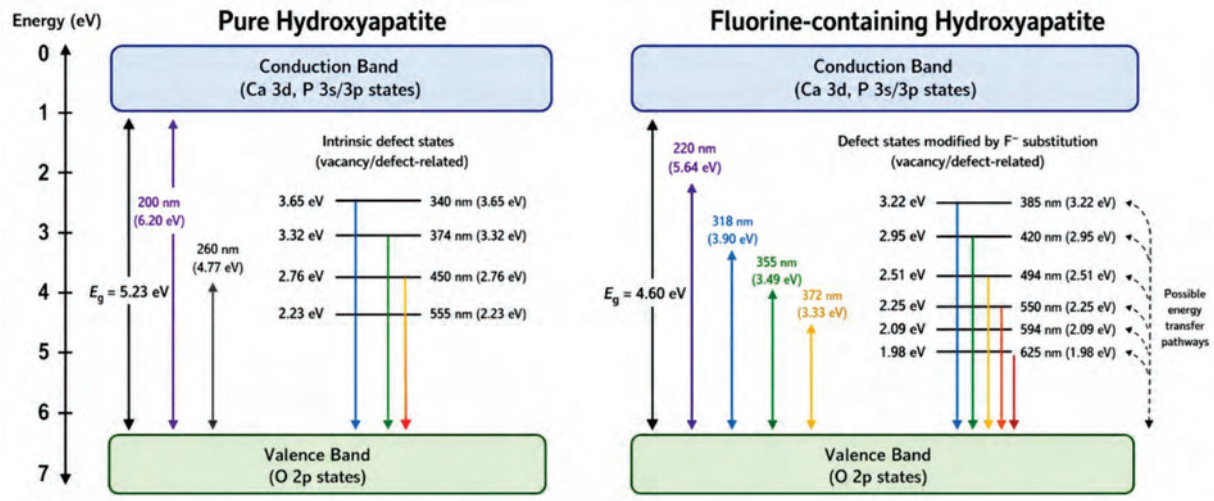

Figure 16. Band diagram of energy levels

associated with defect-related states formed upon fluorine incorporation.

Overall, the spectral results suggest that the incorporation of fluoride ions affects the energy-level structure of HAp, leading to additional excitation and emission bands. This is reflected in the appearance of new spectral features, broadening of the luminescence spectral range, and increased complexity of energy-transfer processes between localized states.

To better understand the luminescence behavior of the samples, the excitation and emission wavelengths were converted into photon energies using the equation $E = 1240/\lambda$, where E is the photon energy in eV and λ is the wavelength in nm (Table 3). For pure HAp, excitation at 200 nm corresponds to an energy of approximately 6.20 eV, while the emission bands at 340 and 450 nm correspond to 3.65 and 2.76 eV respectively. Under excitation at 260 nm, with an excitation energy of 4.77 eV, emission bands at 374, 450, and 555 nm correspond to 3.32, 2.76, and 2.23 eV, respectively. These results indicate that the luminescence of HAp is associated with relaxation from high-energy excited states to lower-energy defect-related states.

For the HAp–F sample, excitation at 220 nm corresponds to 5.64 eV, while the observed emission bands at 385, 494, 550, 594, and 625 nm correspond to 3.22, 2.51, 2.25, 2.09, and 1.98 eV, respectively. The appearance of several emission bands over a wide spectral range indicates that fluorine incorporation modifies the defect structure of hydroxyapatite and creates additional localized energy states. These states may act as radiative recombination centers and contribute to the more complex luminescence behavior of HAp–F compared with pure HAp.

The emission bands observed for HAp–F under excitation at 318, 355, and 372 nm are mainly located around 420 and 550 nm, corresponding to emission energies of approximately 2.95 and 2.25 eV. The repeated appearance of these bands under different excitation wavelengths suggests the presence of stable defect-related luminescence centers. The band near 420 nm may be associated with blue emission from shallow defect levels, whereas the band near 550 nm may correspond to deeper defect states or energy-transfer processes involving fluoride-modified local environments.

Figure 16 shows proposed energy-level diagram and energy-transfer pathways for pure hydroxyapatite (HAp) and fluorine-containing hydroxyapatite (HAp–F). The scheme shows excitation transitions, defect-related energy levels, radiative emission pathways, and possible non-radiative energy transfer between localized states. In pure HAp, luminescence is mainly associated with intrinsic defect states, including oxygen vacancies, hydroxyl vacancies, and PO_4^{3-}-related localized states. In HAp–F, fluorine incorporation modifies the defect structure, de-

Table 3. Calculation of the energies of the main bands

Sample	Excitation, nm	Excitation energy, eV	Emission maxima, nm	Emission energy, eV
HAp	200	6.20	340, 450	3.65, 2.76
HAp	260	4.77	374, 450, 555	3.32, 2.76, 2.23
HAp–F	220	5.64	385, 494, 550, 594, 625	3.22, 2.51, 2.25, 2.09, 1.98
HAp–F	318	3.90	420, 550	2.95, 2.25
HAp–F	355	3.49	420, 550	2.95, 2.25
HAp–F	372	3.33	420, 550	2.95, 2.25

creases the band gap from 5.23 to 4.60 eV, and introduces additional localized states that promote cascade-like energy-transfer processes and broaden the emission range.

Conclusion

This article presents a comparative study of pure and fluorine-containing hydroxyapatite (HAp and HAp–F). Sample synthesis followed by X-ray diffraction (XRD) analysis showed that both materials exhibit the hexagonal apatite-type structure ($P6_3/m$). The observed peak shifts in HAp–F suggest changes in interplanar distances associated with the incorporation of fluorine, without disrupting the overall lattice symmetry. Infrared (IR) spectroscopy revealed spectral changes consistent with fluorine incorporation into the apatite structure, possible partial substitution of OH^- groups by F^- ions, and partial carbonation of the material.

The excitation and emission spectra revealed differences in the luminescent properties of HAp and HAp–F. Fluorine-containing hydroxyapatite exhibits changes in the visible luminescence region, including band broadening and possible modification of defect-related electronic states and energy-transfer processes.

Overall, the findings suggest that the incorporation of fluorine affects the structural and optical properties of hydroxyapatite. These results may provide a basis for further studies of fluorine-containing apatite-based materials for biomedical and luminescent applications.

This research was funded by the Science Committee of the Ministry of Science and Higher Education of the Republic of Kazakhstan (Grant No. AP22788773)

References

1. Abbasi, M., Rashnavadi, M., Gholami, M., & Molaei, S. (2025). Antibacterial property of hydroxyapatite extracted from biological sources and doped with Cu2+ and Ag+ by Sol-gels method. Scientific Reports, 15(1), 12101.
2. Abdulhussein, H. J., Mohsin, M. H., Jabir, M. S., Sulaiman, G. M., Mohammed, H. A., Ismail, R. A., ... & Badher, N. S. (2025). Eco-friendly synthesis of eggshell-derived nano-hydroxyapatite: physicochemical characterization, hemocompatibility, and bone regeneration potential. *Scientific Reports*, *15*(1), 32832.
3. Noori, A., Hoseinpour, M., Kolivand, S., Lotfibakhshaiesh, N., Ebrahimi-Barough, S., Ai, J., & Azami, M. (2024). Exploring the various effects of Cu doping in hydroxyapatite nanoparticle. *Scientific reports*, *14*(1), 3421.
4. Safari-Gezaz, M., Parhizkar, M., & Asghari, E. (2025). Effect of cobalt ions doping on morphology and electrochemical properties of hydroxyapatite coatings for biomedical applications. *Scientific Reports*, *15*(1), 149.
5. Kubiak-Mihkelsoo, Z., Kostrzębska, A., Błaszczyszyn, A., Pitułaj, A., Dominiak, M., Gedrange, T., ... & Hadzik, J. (2025). Ionic doping of hydroxyapatite for bone regeneration: Advances in structure and properties over two decades—a narrative review. *Applied Sciences*, *15*(3), 1108.
6. Arcos, D., & Vallet-Regí, M. (2020). Substituted hydroxyapatite coatings of bone implants. *Journal of Materials Chemistry B*, *8*(9), 1781-1800.
7. Huang, L. H., Sun, X. Y., & Ouyang, J. M. (2019). Shape-dependent toxicity and mineralization of hydroxyapatite nanoparticles in A7R5 aortic smooth muscle cells. *Scientific reports*, *9*(1), 18979.
8. Dudek, J., Faidt, T., Fecher-Trost, C., Thangamurugan, S., Bayenat, P., Trautmann, S., ... & Hannig, M. (2025). Synthetic hydroxyapatite: a perfect substitute for dental enamel in biofilm formation studies. *Scientific Reports*.
9. Rabiei, M., Palevicius, A., Monshi, A., Nasiri, S., Vilkauskas, A., & Janusas, G. (2020). Comparing methods for calculating nano crystal size of natural hydroxyapatite using X-ray diffraction. *Nanomaterials*, *10*(9), 1627.
10. Xiong, X., Li, A., Zhang, Z., Wang, Z., Chen, H., & Guo, L. (2025). In vitro study on the bacteriostatic effect of Amoxicillin-loaded Nano-hydroxyapatite and its capability in occluding dentinal tubules. *Scientific Reports*, *15*(1), 41211.
11. Yan, X., Ebrahimi, A., Mohammadi, R., Tehrani, M. M., Chaboki, P., Mustafa, M., ... & Yousefi, M. (2025). Investigation of bioactivity, biocompatibility, and antibacterial properties of a hydroxyapatite-enhanced nanocomposite for dental applications. *Scientific Reports*, *15*(1), 28557.
12. Eldeeb, G. M., Yousef, M. I., Helmy, Y. M., Aboudeya, H. M., Mahmoud, S. A., & Kamel, M. A. (2024). The protective effects of chitosan and curcumin nanoparticles against the hydroxyapatite nanoparticles-induced neurotoxicity in rats. *Scientific Reports*, *14*(1), 21009.
13. Mo, X., Zhang, D., Liu, K., Zhao, X., Li, X., & Wang, W. (2023). Nano-hydroxyapatite composite scaffolds loaded with bioactive factors and drugs for bone tissue engineering. *International journal of molecular sciences*, *24*(2), 1291.
14. Calabrese, G., Genovese, D., Morganti, D., Rizzo, M. G., Sciuto, E. L., Nicotra, G., ... & Conoci, S. (2025). Core-shell silica and fluorogenic hyaluronan nanomaterials in magnesium hydroxyapatite scaffolds for bone regeneration. *Scientific Reports*, *15*(1), 39589.
15. Li, X., Zhu, J., Man, Z., Ao, Y., & Chen, H. (2014). Investigation on the structure and upconversion fluorescence of Yb3+/Ho3+ co-doped fluorapatite crystals for potential biomedical applications. *Scientific Reports*, *4*(1), 4446.
16. Unnikrishnan, G., Joy, A., Megha, M., Kolanthai, E., & Senthilkumar, M. (2023). Exploration of inorganic nanoparticles for revolutionary drug delivery applications: a critical review. *Discover Nano*, *18*(1), 157.
17. Ielo, I., Calabrese, G., De Luca, G., & Conoci, S. (2022). Recent advances in hydroxyapatite-based biocomposites for bone tissue regeneration in orthopedics. *International journal of molecular sciences*, *23*(17), 9721.
18. Shuai, C., Yang, W., Feng, P., Peng, S., & Pan, H. (2021). Accelerated degradation of HAP/PLLA bone scaffold by PGA blending facilitates bioactivity and osteoconductivity. *Bioactive Materials*, *6*(2), 490-502.
19. Li, Y., Yang, L., Hou, Y., Zhang, Z., Chen, M., Wang, M., ... & Lu, X. (2022). Polydopamine-mediated graphene oxide and nanohydroxyapatite-incorporated conductive scaffold with an immunomodulatory ability accelerates periodontal bone regeneration in diabetes. *Bioactive materials*, *18*, 213-227.

20. Shi, H., Zhou, Z., Li, W., Fan, Y., Li, Z., & Wei, J. (2021). Hydroxyapatite based materials for bone tissue engineering: A brief and comprehensive introduction. *Crystals*, *11*(2), 149.

ИССЛЕДОВАНИЕ ЛЮМИНЕСЦЕНТНЫХ ХАРАКТЕРИСТИК ЧИСТОГО И ФТОРСОДЕРЖАЩЕГО БИОГИДРОКСИАПАТИТА

К. Б. Жанылысов , Д. Х. Дауренбеков , Т. Т. Алибай, Г. Б. Байрбаева, А. С. Ахметова, Р. К. Дауренбекова, Б. Н. Юсупбекова, Е. Г. Кошкинбаев, А. Талгатулы*

Евразийский национальный университет имени Л.Н. Гумилева

** E-mail для контактов: adil.talgatuly.00@gmail.com*

В работе представлено сравнительное исследование чистого и фторсодержащего гидроксиапатита (HAp и HAp–F), направленное на изучение влияния фторид-ионов на структурные и оптические свойства материала. Образцы были получены методом быстрого пиролиза и исследованы с использованием рентгеновской дифракции (XRD), инфракрасной спектроскопии с преобразованием Фурье (FTIR) и люминесцентной спектроскопии. Результаты рентгеновского анализа показали, что оба материала кристаллизуются в гексагональной структуре апатитового типа с пространственной группой $P6_3/m$. Данные FTIR- и XRD-анализа указывают на структурные изменения, связанные с частичным внедрением ионов F^- и изменением локального окружения фосфатных групп. Спектральные и люминесцентные исследования показали, что присутствие фтора влияет на люминесцентные свойства материала, включая изменения в видимой области спектра и возможную модификацию процессов переноса энергии. В целом полученные результаты показывают, что введение фтора влияет на структурные и оптические свойства гидроксиапатита и может служить основой для дальнейших исследований апатитовых материалов для биомедицинских и люминесцентных применений.

Ключевые слова: *Гидроксиапатит; гидроксиапатит, модифицированный фтором; фторгидроксиапатит; инфракрасная спектроскопия; рентгеновская дифракция; сканирующая электронная микроскопия; элементный анализ; фотолюминесценция.*

ТАЗА ЖӘНЕ ФТОРҚҰРАМДЫ БИОГИДРОКСИАПАТИТТІҢ ЛЮМИНЕСЦЕНТТІК СИПАТТАМАЛАРЫН ЗЕРТТЕУ

К. Б. Жанылысов, Д. Х. Дауренбеков, Т. Т. Алибай, Г. Б. Байрбаева, А. С. Ахметова, Р. К. Дауренбекова, Б. Н. Юсупбекова, Е. Г. Кошкинбаев, Ә. Талғатұлы*

Л. Н. Гумилев атындағы Еуразия ұлттық университеті, Астана, Қазақстан

** Байланыс үшін E-mail: adil.talgatuly.00@gmail.com*

Бұл жұмыста таза және фторқұрамды гидроксиапатитке (HAp және HAp–F) салыстырмалы зерттеу жүргізіліп, фторид иондарының материалдың құрылымдық және оптикалық қасиеттеріне әсері қарастырылды. Үлгілер жылдам пиролиз әдісімен алынып, рентгендік дифракция (XRD), Фурье түрлендірулі инфрақызыл спектроскопия (FTIR) және люминесценттік спектроскопия әдістерімен зерттелді. Рентгендік талдау нәтижелері екі материалдың да $P6_3/m$ кеңістіктік тобына жататын гексагоналды апатиттік құрылымда кристалданатынын көрсетті. FTIR және XRD деректері F^- иондарының ішінара енгізілуімен және фосфат топтарының жергілікті ортасының өзгеруімен байланысты құрылымдық өзгерістерді көрсетеді. Спектрлік және люминесценттік өлшеулер фтордың болуы материалдың люминесценттік қасиеттеріне, соның ішінде спектрдің көрінетін аймағындағы өзгерістерге және энергия тасымалдау үдерістерінің ықтимал түрленуіне әсер ететінін көрсетті. Жалпы алғанда, алынған нәтижелер фтордың енгізілуі гидроксиапатиттің құрылымдық және оптикалық қасиеттеріне әсер ететінін және апатит негізіндегі материалдарды биомедициналық және люминесценттік қолдану үшін одан әрі зерттеуге негіз бола алатынын көрсетеді.

Түйін сөздер: *гидроксиапатит, фтормен модификацияланған гидроксиапатит, фторгидроксиапатит, инфрақызыл спектроскопия, рентгендік дифракция, сканерлеуші электрондық микроскопия, элементтік талдау, фотолюминесценция*